


RESEARCH ARTICLE

Open Access



Unsinkable, long-drifting, millimeter-sized pumice of the 2021 eruption of Fukutoku-Oka-no-Ba submarine volcano

Shingo Takeuchi^{1*} , Kosuke Ishige¹, Shimpei Uesawa¹ and Yukiko Suwa²

Abstract

Understanding the relationship between pumice formation and long-term floatability in seawater is becoming increasingly important in terms of eruption dynamics, material cycles, biological and environmental effects, and ocean hazards. Pumice rafts were produced during the 2021 eruption of the Fukutoku-Oka-no-Ba submarine volcano in the Pacific Ocean, far from the Japanese archipelago. The pumice rafts reached the Amami-Ōshima and Okinawa Islands approximately two months after the eruption and continued to cover the sea surface at several bays and ports, providing a great opportunity to study the characteristics of raft pumices. Sieve analysis of the floating pumice indicated that the pumice rafts characteristically contained several millimeter-sized particles with a peak at 2–4 mm. This evidence raises an important question why the millimeter-sized, Fukutoku-Oka-no-Ba 2021 pumice particles were able to float for over two months, which exceeds the floatation time shown in previous studies. To answer this question, a porosity measurement technique for millimeter-to-centimeter-sized pumice particles was established and applied to drifting pumice that erupted during the Fukutoku-Oka-no-Ba 2021 eruption. The total, connected, and isolated porosities (including errors) were acquired for floating and sunken pumice particles. As studied for the floating pumice from past submarine eruptions, most floating pumice particles contain a high amount of isolated porosity (> 30 vol%) and are thus unsinkable even when the pumice size is in the millimeter scale. This study emphasizes that skeletal density is a useful measure for the determination of pumice floatability (sinkable or unsinkable). As the particle size decreases, crystals are lost from the floating pumice particles, suggesting that the particle size of the floating pumice is affected by its petrological properties (crystal content and size). A comparison with natural pumices from subaerial eruptions and experimental pumices from magma decompression experiments suggests that the Fukutoku-Oka-no-Ba 2021 pumices contain abundant isolated pores due to the suppression of expansion after fragmentation by quenching in seawater, and that the relatively low to moderate crystal content in the magma (< 17 vol%) may contribute to favorable conditions to produce abundant, millimeter-sized, unsinkable pumice.

Keywords 2021 Fukutoku-Oka-no-Ba volcano eruption, Pumice raft, Porosimetry, Connected and isolated porosity, Unsinkable pumice

1 Introduction

Pumice is a highly porous, glassy volcanic rock produced by magma vesiculation and quenching during volcanic eruptions. Pumice sometimes has a lower density than water, producing floatability in water. In addition to volcanic ash dispersion in the atmosphere, pumice transport by water flow on land and in the ocean causes

*Correspondence:

Shingo Takeuchi
takeshin@criepi.denken.or.jp

¹ Nuclear Risk Research Center, Central Research Institute of Electric Power Industry, 1646 Abiko, Abiko, Chiba 270-1194, Japan

² CERES, Inc., SEC Building 4F, 5-6-13 Namiki, Abiko, Chiba 270-1165, Japan

widespread dispersion of volcanic materials to extensive areas. Recent advances in satellite imagery have revealed the common occurrence of drifting pumice rafts that have erupted from submarine volcanoes (e.g., Jutzeler et al. 2014, 2020). An analysis of old document records also has revealed the history of drifting pumice washed ashore along the Nansei Islands, Southwest Japan, since the eighteenth century (Oikawa et al. 2023). In some cases, drifting pumices float on the sea surface for distances of thousands of kilometers. (e.g., Bryan et al. 2012). Therefore, understanding the relationship between pumice formation and long-term floatability in seawater is becoming increasingly important in terms of eruption dynamics, material cycles, biological and environmental effects, and ocean hazards.

Drifting pumice rafts occurred during the 2021 eruption of Fukutoku-Oka-no-Ba (hereafter referred to as FOB) submarine volcano in the Pacific Ocean, far from

the Japanese archipelago (Fig. 1a). The 2021 FOB eruption and drifting pumice rafts have been extensively studied. Despite the submarine volcanoes being far from land, the time evolution of the 2021 eruption has been recorded using high-resolution satellite images (Maeno et al. 2022; Fauria et al. 2023), infrasound remote observations (Maeno et al. 2022), and ionospheric response observations (Heki and Fujimoto 2022). Pumice rafts drifting on the sea surface have been observed using high-resolution satellite images (Kaneta and Chiba 2022; Maeno et al. 2022; Fauria et al. 2023; Iskandar et al. 2023). The pumice rafts drifted thousands of kilometers and reached the Amami-Ōshima and Okinawa Islands approximately two months after the eruption and then reached the coast of Southeast Asia several months later (Yoshida et al. 2022a). The arrival times of drifting pumice washed onto beaches have been recorded in detail in several previous studies (Konoo et al. 2022; Usami and

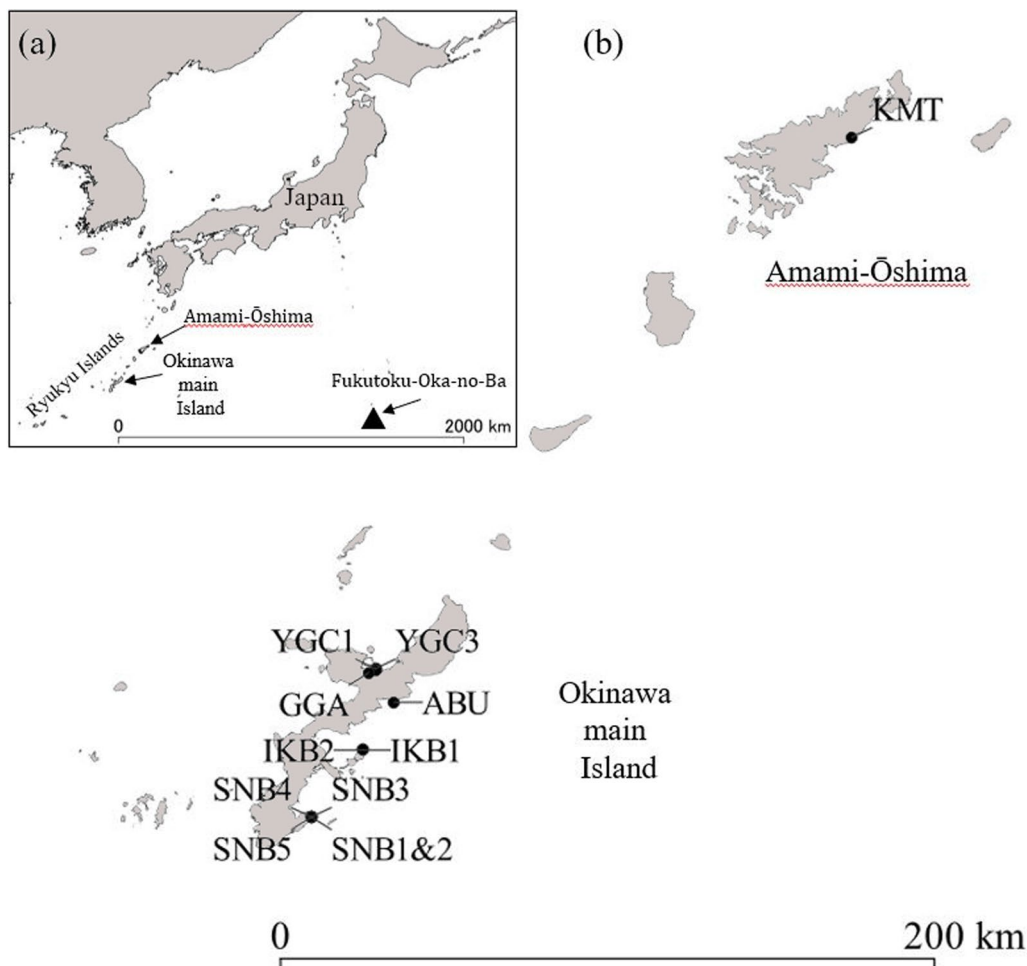


Fig. 1 **a** Location of the Fukutoku-Oka-no-Ba volcano in the Izu-Bonin Islands and Okinawa main and Amami-Ōshima Islands. **b** Sampling localities in Okinawa main and Amami-Ōshima Islands

Shinjo 2022; Yoshida et al. 2022a, b, c). Awareness of this phenomenon has motivated simulation studies on drifting pumice rafts from the FOB and other volcanoes (Shiraki et al. 2022; Asami and Takahashi 2023; Chang et al. 2023; Nishikawa et al. 2023; Iskandar et al. 2023). Petrological studies on pumice of FOB 2021 have focused on the eruption process from the magma chamber to the atmosphere (Maeno et al. 2022; Yoshida et al. 2022b, 2023a). Drifting pumice has impacted coastal environments and human societies. The effects of drifting and beached pumices on coastal vegetation and aquatic life have also been observed (Ohno et al. 2022; Akiyama et al. 2022; Sato et al. 2023). Vessels and fishing industries have suffered severe damage from drifting pumices. The high proportion of millimeter-sized pumice particles, which is a notable feature of the pumice rafts of FOB 2021 as shown in Sect. 6.1, were sucked into the cooling system of vessels or into the bodies of cultured fish that mistook the pumice particles for bait (Ohno et al. 2022). Fishing was halted to avoid vessel breakdown, increasing economic damage (Ryukyu Shimpō 2021). The behavior of floating pumice in ports with various types of breakwaters has been observed from the viewpoint of port engineering (Nagayama and Izaki 2022; Nakata et al. 2022; Noshi et al. 2022; Takahashi et al. 2022). Floating pumice in ports were removed to reduce the impact on vessels, and the removal cost exceeded 1.6 billion yen as of February 2022 (Ryukyu Shimpō 2022).

Previous experimental and modeling studies on floating pumices have shown that the floatation time is related to the particle size (Whitham and Sparks 1986; Manville et al. 1998; Fauria et al. 2017). The larger the pumice particles, the longer they float. Manville et al. (1998) revealed that < 4 mm-sized pumice particles can sink within two months. This knowledge raises an important question why the millimeter-sized, FOB 2021 pumice particles were able to float for over 2 months. The key to solving this question lies in the porosimetric characteristics of the floating pumice. Previous studies on drifting pumices have revealed that they contain abundant isolated pores, which enable them to float eternally (Kato 1987, 1988; Manga et al. 2018; Mitchell et al. 2021), hereafter referred to as unsinkable pumice. This feature significantly differs from pumices from subaerial explosive eruptions, which have been the main experimental samples for previous studies on pumice floatation (Whitham and Sparks 1986; Manville et al. 1998; Fauria et al. 2017). Although pumices from subaerial eruptions have high porosity, they also have high pore connectivity on average, resulting in low isolated porosity (Colombier et al. 2017a). Based on these previous studies, drifting pumice from the FOB 2021 eruption is a valuable case to study particle size and floating features for precise porosimetry.

In this study, we sampled floating pumice on the sea surface near the land and quantified their particle size characteristics. Subsequently, we developed methods of porosity measurement for millimeter- to centimeter-sized pumice particles and obtained the total, connected, and isolated porosities over a wide range of particle sizes. Finally, we discuss the floatability of the pumice and its relationship with petrological and magmatic features.

2 Definitions of terms

In this study, we discuss various pumice states. To facilitate clarity and understanding, we have defined the terms used in this study as follows. Because this study focuses on long-drifting pumice, these definitions are for cold pumice.

Pumice raft: Pumice particles floating in clusters on the sea surface.

Floating pumice: Pumice particles floating on the sea surface, including both unsinkable and sinkable pumice.

Sunken pumice: Pumice particles that have sunken in the seawater.

Beached pumice: Pumice particles washed ashore and deposited on the beach.

Unsinkable pumice: Pumice particles floating on the sea surface and unsinkable when their connected pores are saturated because of their high isolated porosity.

Sinkable pumice: Pumice particles that can eventually sink in seawater, including floating pumice, due to trapped air in the connected pores.

The terms, floating pumice and sunken pumice, are defined as referring to the state at the time of observation. In contrast, the terms, unsinkable pumice and sinkable pumice, are defined as the state in which the connecting pore is saturated with seawater.

3 The 2021 eruption at the Fukutoku-Oka-no-Ba submarine volcano

The FOB is a submarine volcano in the Izu–Bonin volcanic arc, approximately 1300 km south of Tokyo (Fig. 1a), and forms the central cone of the North Fukutoku Caldera (Ito et al. 2011; Minami and Tani 2023). Eruptions, pumice rafts, and discolored water have been frequently observed at the FOB since the beginning of the twentieth century (Minami and Tani 2023). The FOB 1986 eruption was at a large scale and caused drifting pumice that reached the Ryukyu Islands (Kato 1988). In 2010, a seafloor survey revealed that the crater was approximately 30 m below sea level (Ito et al. 2011).

Maeno et al. (2022) analyzed and summarized a time series of the FOB 2021 eruption based on satellite imagery and airborne observations. The eruption began at 05:55 JST on August 13, 2021. The eruption is classified into four phases. Phase 1 produced a continuous

high eruption column with a height of 16 km for approximately 14 h. The plume was notably white. Phase 1 was the most intense, ejecting most of the eruptive product, and the following stages shifted to a relatively less intense pulsating, Surtseyan activity. Pumice rafts were identified in Phase 1 and drifted west–northwest, carried by ocean currents. The estimated volume of the eruptive product from the pumice rafts and new islands around the eruptive vent, likely formed in Phase 1, is 0.1–0.4 km³ (0.03–0.1 km³ dense rock equivalent; Maeno et al. 2022).

4 Drifting pumice of the Fukutoku-Oka-no-Ba 2021 eruption

There is a record of observation of drifting raft pumice made by a research vessel Keifu-Maru of the Japan Meteorological Agency (Japan Meteorological Agency, 2021a, b). The raft pumice was sampled on August 22, 2021, at a location ca. 300 km northwest of the FOB volcano. Although no particle size distribution data are available, it is reported that millimeter- to centimeter-sized pumice was main size in the pumice raft. According to Yoshida et al. (2022b), on October 5, 2021, the pumice rafts drifted west–northwest ca. 1040 km to the Daito Islands and further west–northwest to the Amami-Ōshima and Okinawa Islands after October 10, 2021. In the summer of 2022, pumice drifted to the Pacific Ocean and Sea of

Japan, and beached pumices were reported (Yoshida et al. 2022a). The route taken by the pumice rafts drifting from the FOB volcano to the Amami-Ōshima and Okinawa Islands and the Taiwan Islands was revealed using satellite image analysis (Iskandar et al. 2023).

In the following section, we describe the appearance of pumice rafts observed on the shore. Millimeter-sized pumice particles were spread over the sea surface in a large amount. Underwater and coarser pumice particles were observed underneath a layer of millimeter-sized particles (Yomiuri Shinbun 2021). A similar grading structure was observed when the pumice sample was floated in a laboratory tank (Fig. 2a).

A pumice raft, not constrained by its surroundings, appears to have a relatively lower thickness. The motion of the thin pumice raft followed the wave movements on the sea surface. However, the motion of a pumice raft, pushed onto the shore by the wind and/or ocean currents, is more resistant to wave movement. This resistive behavior is due to the high thickness of the pumice raft, which is increased by lateral stresses from wind and/or currents. A similar response of pumice rafts to wave motion, dependent on layer thickness, has also been observed in high-resolution satellite images for the FOB 2021 eruption (Fauria et al. 2023), and 7 August 2019 pumice raft from the Tonga Arc (Jutzeler et al. 2020).

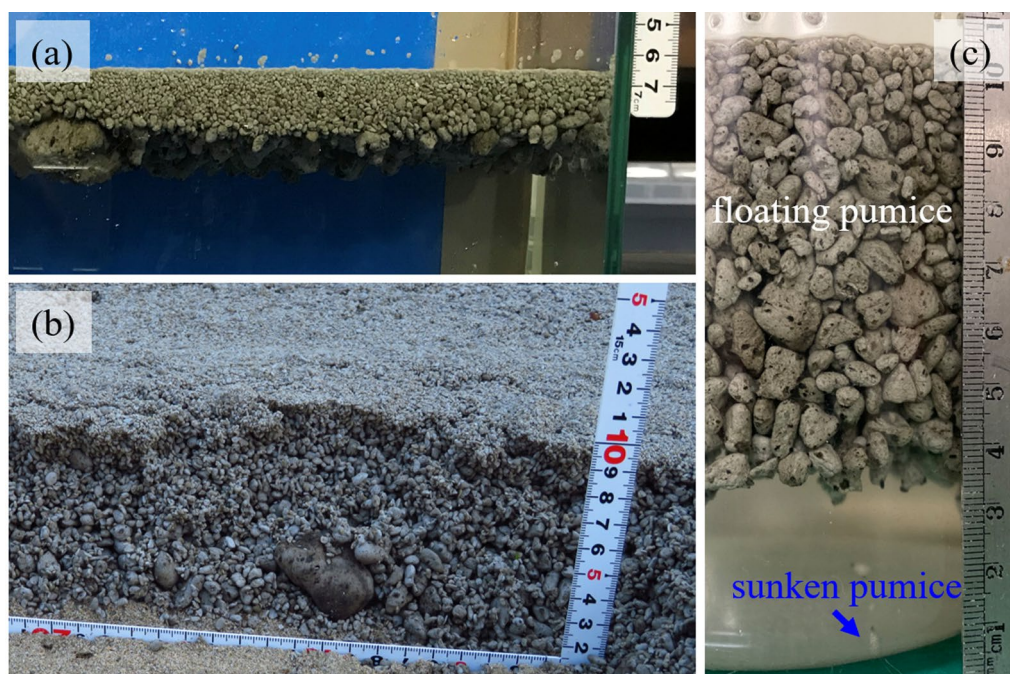


Fig. 2 **a** Grading structure of the floating pumice particles in pumice rafts reproduced in a laboratory tank. **b** Grading structure of the beached pumice deposit at the coast facing Haneji-Naikai in the Okinawa main Island. **c** Floating and sunken pumices in a container with artificial seawater. This image was taken on December 15, 2023, more than two years after it was sampled from the sea surface and began to be stored in the container with seawater

Under lateral stress, the upper part of the pumice raft is lifted above the sea surface because of the buoyancy of the thicker underwater part. The particles in the upper part of the raft were in contact with each other in the air. The more intense mechanical interaction between the pumice particles in the air can produce a higher yield strength in the upper part of the pumice raft. The yield strength of thick pumice rafts is evidenced by the presence of small objects on them, such as crabs (Akiyama et al. 2022).

The appearance of beached pumice deposits depends on the amount of pumice, beach orientation, and direction of wind and currents (Yoshida et al. 2022b). Cross-sections of a massive, beached pumice deposit in the inland sea, where the waves were calm, showed a grading structure (Fig. 2b) similar to that observed in the sea (Yomiuri Shinbun 2021) and in the tank (Fig. 2a). Beached pumice deposits returned to the sea during high tide. Therefore, the sampled pumices from the sea surface near the shore in this study might not float on the sea surface for the entire period from eruption to sampling and have been washed ashore several times.

Pumice rafts from the FOB 2021 eruption contain various petrological types of pumice. Yoshida et al. (2022b) classified pumice into six types based on color and texture. The most abundant type (>90%) was gray pumice. The other minor types were black, brown, pale gray, amber, and streaky. The gray pumice consists of a gray vesicular groundmass and phenocrysts.

5 Methods

5.1 Sampling

In this study, pumices were sampled from the sea surface to determine the particle size distribution of floating pumice in pumice rafts. The sampling locations and dates are shown in Fig. 1b and Table 1. Two methods were adopted to collect floating pumice samples: scooping pumice particles with seawater using a container (IKB1, SNB1&2, and SNB3), and scooping pumice particles using a sieve or pole net (IKB2, YGC1, and YGC3). In the former method, a submerged container was quickly lifted to sample floating pumice on the sea surface of shallow water near the shore. In the latter method, a collector lowered a sieve with a 500–800 μm mesh opening and a diameter of 18.5 cm from a bridge over an inland sea. The sieve was submerged in the sea and quickly lifted to sample the floating pumice. Instead of the sieve, a pole net with a 200–350 μm mesh opening and a diameter of 27 cm was extended from the shore to sample floating pumice on the sea surface. Some pumice samples were collected from floating pumice (GGA and MKY) or beached pumice deposits (ABU, SNB4,

Table 1 Sampling locality and date, sample appearance and sampling method

Name	Latitude	Longitude	Sampling date	Appearance	Method ^a
ABU	26.5384	128.0921	19-Oct-21	Beached	HS
IKB1	26.3877	127.9910	20-Oct-21	Floating	C
IKB2	26.3877	127.9910	20-Oct-21	Floating	PN
KMT	28.3197	129.5356	27-Oct to 1-Nov-21	Floating	PS ^b
YGC1	26.6445	128.0327	01-Nov-21	Floating	S
YGC3	26.6445	128.0327	01-Nov-21	Floating	S
SNB1&2	26.1763	127.8307	03-Nov-21	Floating	C
SNB3	26.1763	127.8307	03-Nov-21	Floating	C
SNB4	26.1763	127.8307	03-Nov-21	Beached	HS
MKY	26.6373	128.0348	08-Mar-22	Floating	HS
GGA	26.6318	128.0117	08-Mar-22	Floating	HS
SNB5	26.1763	127.8307	10-Mar-22	Beached	HS

^a Pumice scooped by a container with seawater (C), a hand shovel (HS), a pole net (PN), a power shovel (PS) and a sieve (S)

^b Pumice removed for port restoration was acquired from port officials

and SNB5) to obtain sufficient samples or large particles. A sample of pumice removed for port restoration was acquired from port officials (KMT). The samples were lifted with the seawater (IKB1, SNB1&2, and SNB3) and stored with seawater in the laboratory. We reproduced the floating of a sample lifted using a pole net (IKB2) in a laboratory tank containing artificial seawater. The pumice particles floated at the time of sampling; however, over time, a small number of pumice particles sank to the bottom of the container (Fig. 2c). Such pumices were termed sunken pumices and were also analyzed. Samples of IKB1, SNB1&2, SNB3 and IKB2 were stored in containers with seawater for the duration of 16, 15, 13 and 35 days, respectively. Pumice particles in these samples were then determined whether floating or sunken and prepared for density measurements. GGA, MKY and YGC3 were sampled as floating pumice at the time of sampling in the field. All particles used for the measurements in this study were gray pumice, as classified by Yoshida et al. (2022b) and Konoo et al. (2022). Density measurements were performed on samples in the natural state of the pumice particles without shaping or processing.

Large pumice particles for the polished sections (1103-5C-GP1, AB3a-Tim1_V, and AB3a-Tim1_P) were sampled from beached pumice deposits (SNB5 and ABU) in addition to the sections (AM12-1 and AM12-2) of pumices provided by port officials (KMT). After resin impregnation to pores by using a vacuum, the polished sections of pumice were produced.

5.2 Particle size analysis

Sieving of the sampled floating pumices was performed to obtain their particle size distributions on a Φ scale at an interval of 0.5 Φ . The Φ scale is defined as $\Phi = -\log_2 D/D_0$, where D and D_0 are the particle diameter (mesh opening) in millimeters and the reference diameter (1 mm), respectively (Krumbein 1934; McManus 1963). Before sieving, the samples were soaked in tap water for one to several days and dried at 110 °C in an oven. A low quantity of impurities (plant fragments and seaweed) were removed during soaking and drying. Any particles that sank during soaking in tap water were collected to avoid loss. Dried samples with an initial mass of 40–500 g were manually sieved. Completeness of sieving down to -1Φ (2 mm in particle diameter) was confirmed by the naked eye. The samples were then sieved using a shaking sieve system with an electromagnetic drive (Vibratory Sieve Shaker ANALYSETTE 3 PRO, Fritsch GmbH), with the smallest vibration amplitude (0.5 mm). Through a time run with several time intervals, ranging from several tens of seconds to several minutes, the end of the sieve analysis was determined by checking for a mass change of each sieve class within 1% of the initial sample mass.

5.3 Porosimetry

In this section, the density measurement methods are briefly summarized. The details of the measurements using gas and pseudofluid displacement methods are described in the Supplementary Materials.

5.3.1 Definition and calculation of porosity

Considering the porosimetric properties of pumice particles, the total porosity, connected porosity, and isolated porosity of pumice particles are defined (e.g., Yokoyama and Takeuchi 2009). Pores that are opened to the outside and closed inside a pumice particle are called connected and isolated pores, respectively. The volume fractions of the connected and isolated pores in the volume of the pumice particle are defined as connected and isolated porosities, respectively. The total porosity is the sum of connected and isolated porosities.

Porosity was calculated based on the measured densities of the samples. For porosity calculation, the density of the gas filling the pores was assumed to be zero because it is negligible compared to the solid density. The solid density, ρ_s , is the density of the solid phase in a pumice particle consisting of crystals and glass. Bulk density, ρ_b , is the density of a pumice particle consisting of the solid phase and the total pores. Skeletal density, ρ_{s+i} , is the density of the combined portions of solid phase and isolated pores inside the pumice particle (e.g., Michol et al. 2008). The skeletal density is useful because it is the

primary density output in the measurement of the gas displacement method (Sect. 5.3.3).

Following Michol et al. (2008), the total porosity, ϕ_t , is calculated using the bulk and solid densities as follows:

$$\phi_t = 1 - \frac{\rho_b}{\rho_s} \quad (1)$$

The connected porosity, ϕ_c , is calculated using the bulk and skeletal densities as follows:

$$\phi_c = 1 - \frac{\rho_b}{\rho_{s+i}} \quad (2)$$

The following relationship exists among total, connected, and isolated porosities, ϕ_i :

$$\phi_t = \phi_c + \phi_i \quad (3)$$

5.3.2 Measurement of bulk density

Volume measurement is a significant hurdle in obtaining the bulk density of pumice particles. The Archimedes' method is the simplest for measuring the volume of an object. However, the Archimedes' method cannot measure the volume of pumice particles with connected pores into which water can infiltrate. To overcome this technical hurdle, several methods for the surface coating of pumice particles have been proposed (e.g., Houghton and Wilson 1989). The pseudofluid displacement method is also effective in measuring the volume of porous materials such as pumice. In the pseudofluid displacement method, a sample is placed in a container with a pseudofluid such as glass beads. The volumes change before and after sample placement are measured. The glass beads method (Sasaki and Katsui 1981) is well known in volcanology and is used to measure the bulk density of pyroclasts (Shimano and Nakada 2006; Nakamura et al. 2008; Colombier et al. 2017b). It was assumed that the pseudofluid does not infiltrate the connected pores of the pumice particles. Recently, a precise volume measurement instrument (GeoPyc 1365, Micromeritics) has enabled us to measure volumes using the pseudofluid displacement method and has been used in volcanology (e.g., Pardo et al. 2012; Heinrich et al. 2020). In this study, the volume of the pumice particles was measured using a GeoPyc 1365 installed at the Central Research Institute of Electric Power Industry. A dedicated DryFlo powder (40–280 μm in particle diameter) and FGB40 glass beads (355–500 μm in particle diameter) were used as the working pseudofluids, whose details are described in Section S1.2 in the Supplementary Materials. While measurements in previous volcanological studies have often been conducted on centimeter-sized particles, we here measured millimeter-sized particles. Volumetric

measurement methods were divided into measurements for a single-particle sample if the volume of a particle was $>0.1 \text{ cm}^3$ and measurements for a multiparticle sample if the volume of a particle was $<0.1 \text{ cm}^3$. In the multiparticle sample measurements, the average volume and density of the multiparticles were measured. The validity of the measurements using GeoPyc 1365 was examined based on a comparison with values from the Archimedes' method, and thus, non-porous reference objects of various shapes and volumes from millimeters to centimeters in size were measured (Tables S2 and S3). Based on this comparison, we corrected the systematic errors observed in the measurements of a single-particle sample with $<1 \text{ cm}^3$ and multiparticles. Eventually, we concluded that the bulk density measurements in this study had maximum relative errors of 3 and 5% for single- and multiparticle samples, respectively (Figs. S1 and S2). The larger the sample volume, the smaller the relative error in the bulk density measurement of 1.5%.

5.3.3 Measurement of skeletal density

In volcanology, gas displacement method (gas pycnometry) is the standard method for measuring the skeletal density of porous volcanic materials. The skeletal volume, defined as the sample mass divided by the skeletal density measured by the gas displacement method, does not include the connected pores through which the working gas can enter and exit. In this study, the skeletal volume of the pumice particles was measured using a Quantachrome Penta-Pycnometer at the Central Research Institute of Electric Power Industry. Helium was used as the working gas. As well as the pseudofluid displacement method, we examined the validity of density measurements in the gas displacement method for small objects by comparing the volume values of non-porous, small objects obtained using the Archimedes' method. We evaluated the volume detection limit to 0.1 cm^3 (Fig. S3a). The maximum relative error of the skeletal density measurements was 40% for 0.1 cm^3 in skeletal volume. The larger the skeletal volume, the smaller the relative error in skeletal density measurement at $<1\%$ (Fig. S3a, b and c). The error in gas displacement method depends mostly on the volume of sample compared to the volume of the cell used. The same criteria for bulk density measurements were used to classify measurements of single- and multiparticle samples.

5.3.4 Measurement of solid density

Solid density was measured for a sufficiently pulverized powder of pumice particles using the gas displacement method, a Quantachrome Penta-Pycnometer at the Central Research Institute of Electric Power Industry. The powdered samples used for solid density measurements

were the same as those prepared for X-ray fluorescence (XRF) analyses. Solid density measurements were difficult to obtain for sunken pumice because a sufficient amount of sieved samples could not be obtained. Therefore, the relationship between the solid density and particle volume of floating pumice was also applied to sunken pumice. The relative error of the solid density measurement was evaluated based on the sample volume using the same functions as for the skeletal density measurement using the gas displacement method (Section S1.3).

5.4 Petrological analysis

As shown in Sect. 6.4 later, we observed a change in solid density with particle size. To examine the change in solid density in terms of change in crystal content, we estimated crystal size and content in pumice by image analysis of elemental and electronic images, and mass balance calculations of the K_2O content among the bulk rock, glass, and crystals, respectively. Methods for image analysis for pumice sections and chemical analysis for bulk rock, glass and crystals are described in the Supplementary Materials.

6 Results

6.1 Particle size distribution

The particle size distributions of the floating pumice samples were obtained from four sites (IKB1, SNB1&2, YGC1, and YGC3; Table 1). There was no significant difference between the sampling methods, particularly with respect to smaller particle sizes (Fig. 3). Results show that the number of particles that escaped through the sieve mesh was negligible. Data from all sites showed a primary peak of -1Φ to -2Φ , that is, 2–4 mm in diameter (Fig. 3). A decrease on the finer side down to 1Φ (0.5 mm

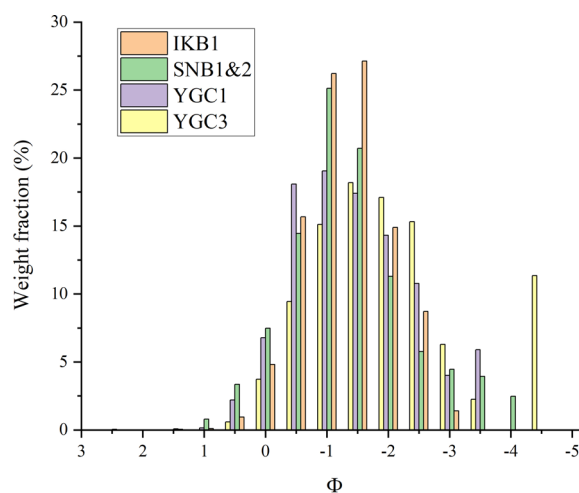


Fig. 3 Particle size distributions of the floating pumice samples

in diameter) was also common. By contrast, samples with or without a second peak on the coarser side were present.

6.2 Bulk density

The bulk densities of all floating pumice particles were below that of the density of seawater (Fig. 4a, Table 2 and Table S1). Floating pumices $>0.1 \text{ cm}^3$, measured as a single-particle sample, have a wide range of bulk densities from 0.2 to 0.8 g/cm^3 at an average of 0.56 g/cm^3 . Floating pumices $<-2.5 \Phi$ (5.6 mm in diameter and 0.095 cm^3 in equivalent sphere volume), measured as a multiparticle sample, have bulk density values decreasing from 0.7 to 0.5 g/cm^3 with decreasing particle volume. However, this decrease was within the density range of particles $>0.1 \text{ cm}^3$. Sunken pumices, measured as single-particle samples $>0.2 \text{ cm}^3$, have bulk densities around 0.6 g/cm^3 overlapping those of floating pumices. Sunken

pumices $<-3.0 \Phi$ (8 mm in diameter and 0.27 cm^3 in equivalent sphere volume), measured as multiparticle samples, have higher bulk densities ($0.7\text{--}0.8 \text{ g/cm}^3$) than those of floating pumice particles with a similar particle volume.

6.3 Skeletal density

The skeletal densities of most floating pumice particles were lower than that of the seawater (Fig. 4b, Table 2 and Table S1). Most floating pumice particles $>0.1 \text{ cm}^3$ have a range of skeletal densities from 0.7 to 1.0 g/cm^3 at an average of 0.88 g/cm^3 . A large floating pumice particle with a skeletal density of 1.2 g/cm^3 higher than that of seawater was found. Floating pumice $<-2.5 \Phi$ (5.6 mm in diameter and 0.095 cm^3 in equivalent sphere volume) tends to have a non-variable skeletal density with decreasing particle volume, which is lower than the density of seawater. Sunken pumices, measured as a single-particle sample, $>0.2 \text{ cm}^3$, have skeletal densities of $1.1\text{--}1.3 \text{ g/cm}^3$; however, some data have large errors owing to the small skeletal volume. These skeletal densities were higher than those of floating pumice particles and seawater. Sunken pumice particles, measured as a multiparticle sample, $<-3.0 \Phi$ (8 mm in diameter and 0.27 cm^3 in equivalent sphere volume) tend to have increasing skeletal densities from 1.1 to 1.4 g/cm^3 with decreasing particle volume. However, notably, the sunken pumice with a diameter of 0 to -1Φ (1–2 mm in diameter and 5.2×10^{-4} to $4.2 \times 10^{-3} \text{ cm}^3$ in equivalent sphere volume) has a large error owing to the small skeletal volume.

6.4 Solid density

Solid densities of the floating pumice monotonously increase from 2.5 to 2.8 g/cm^3 with increasing particle size from 1.0 to -5.5Φ (0.5–45.8 mm in diameter) (Fig. 5a and Table 3). Yoshida et al. (2022b) classified the pumices of FOB 2021 as trachyte (alkaline magma) based on their bulk rock composition. Although there is a large difference in the chemical variation between the alkaline and sub-alkaline magmas, the solid density of the trachyte of FOB 2021 is close to that of andesitic to dacitic rocks (sub-alkaline magma), which have a similar bulk SiO_2 content (Takeuchi et al. 2021). Fitting a linear function with this relationship between solid densities and size in the Φ scale (Fig. 5a), we obtain an empirical linear function that can be used to calculate the relationship between particle volume and solid density for the FOB floating pumice as follows:

$$\rho_s = -0.0413\Phi + 2.51 \tag{4}$$

where Φ is the particle diameter in the Φ scale (Sect. 5.2). In the calculation of solid density using Eq. (4) for

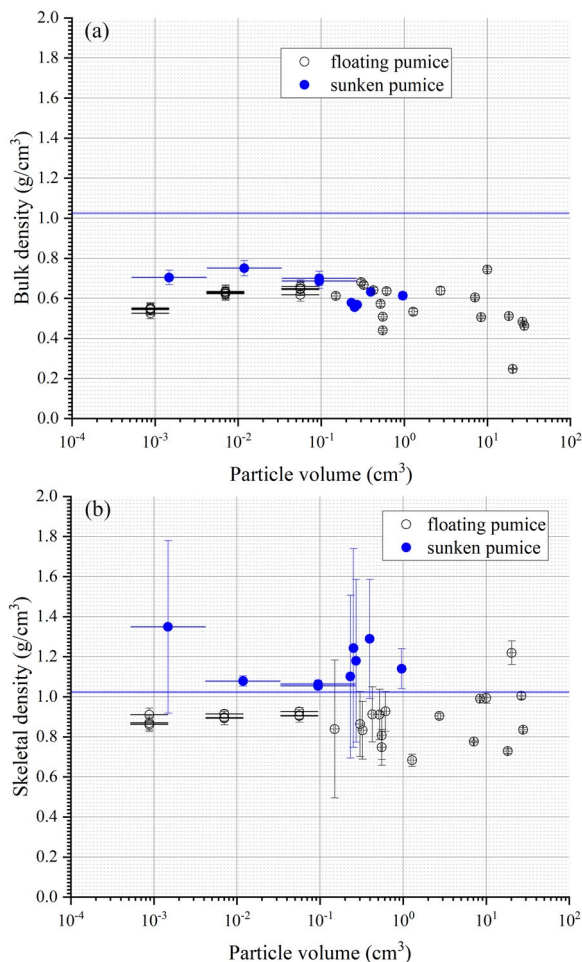


Fig. 4 **a** Bulk density and **b** Skeletal density vs. particle volume. A horizontal blue line indicates an assumed range in the density of seawater ($1.02\text{--}1.03 \text{ g/cm}^3$), based on Wadachi (1987)

Table 2 Porosimetical data of floating and sunken pumice erupted in the Fukutoku-Oka-no-Ba 2021 eruption

Name	Particle volume (cm ³)	Bulk density (g/cm ³)	Skeletal density (g/cm ³)	Solid density (g/cm ³)	Total porosity (vol%)	Connected porosity (vol%)	Isolated porosity (vol%)	Pore connectivity (vol%)	Saturation density (g/cm ³)
<i>Floating pumice^d</i>		0.25–0.74 (0.58)	0.68–1.22 (0.89)	2.52–2.77 (2.62)	73–91 (78)	20–80 (34)	11–58 (44)	27–88 (43)	0.76–1.06 (0.93)
IKB1-flt 4 mm	0.06 ^b	0.62	0.91	2.60	76	32	44	42	0.94
IKB1-flt 2 mm	0.007 ^b	0.63	0.91	2.56	76	32	44	42	0.95
IKB1-flt 2 mm-2	0.007 ^b	0.62	0.91	2.56	76	32	44	42	0.95
IKB1-flt 1 mm	0.0009 ^b	0.55	0.87	2.52	78	37	41	47	0.93
IKB2-flt1	0.52	0.57	0.91	2.65	78	37	41	47	0.95
IKB2-flt4	0.61	0.64	0.93	2.65	76	31	45	41	0.96
IKB2-flt5	0.55	0.44	0.81	2.65	83	45	38	55	0.91
IKB2-flt7	0.43	0.64	0.91	2.64	76	30	46	39	0.95
IKB2-flt8	0.33	0.67	0.83	2.64	75	20	55	27	0.87
IKB2-flt14	0.15	0.61	0.84	2.62	77	27	50	35	0.89
YGC3-flt 4 mm	0.06 ^b	0.66	0.93	2.60	75	29	46	39	0.95
YGC3-flt 4 mm-2	0.06 ^b	0.65	0.93	2.60	75	30	45	40	0.96
YGC3-flt 2 mm	0.007 ^b	0.63	0.90	2.56	75	30	46	39	0.93
YGC3-flt 1 mm	0.0009 ^b	0.54	0.86	2.52	78	37	42	47	0.92
YGC3-flt 1 mm-2	0.0009 ^b	0.53	0.86	2.52	79	39	40	49	0.93
SNB1&2-flt 4 mm	0.06 ^b	0.65	0.90	2.60	75	28	47	38	0.94
SNB1&2-flt 2 mm	0.007 ^b	0.63	0.89	2.56	75	29	46	38	0.93
SNB1&2-flt 1 mm	0.0009 ^b	0.55	0.91	2.52	78	39	39	50	0.96
SNB3-flt1	1.28	0.53	0.68	2.67	80	22	58	27	0.76
SNB3-flt3	7.11	0.60	0.78	2.70	78	22	55	29	0.83
SNB3-flt2	0.30	0.68	0.86	2.64	74	21	53	28	0.90
SNB3-flt5	0.55	0.51	0.75	2.65	81	32	49	40	0.84
SNB3-flt6	10.00	0.74	0.99	2.71	73	25	47	35	1.00
MKY-flt1	8.42	0.51	0.99	2.70	81	49	32	60	1.01
MKY-flt2	2.73	0.64	0.90	2.68	76	29	47	39	0.94
GGA-flt1	20.25	0.25	1.22	2.72	91	80	11	88	1.06
GGA-flt2	18.23	0.51	0.73	2.72	81	30	51	37	0.82
GGA-flt3	27.87	0.46	0.83	2.73	83	45	38	54	0.92
GGA-flt4	26.61	0.48	1.00	2.73	82	52	30	63	1.02
<i>Sunken pumice^a</i>		0.56–0.75 (0.64)	1.05–1.35 (1.17)	N.D. ^c	71–79 (75)	30–55 (44)	24–40 (31)	43–70 (59)	1.04–1.19 (1.10)
IKB1-snk1	0.40	0.63	1.29	2.64	76	51	25	67	1.15
IKB1-snk2	0.23	0.58	1.10	2.63	78	48	31	61	1.06
IKB1-snk4	0.25	0.56	1.24	2.63	79	55	24	70	1.12
IKB2-snk2	0.27	0.57	1.18	2.63	78	52	27	66	1.10
SNB3 snkLb-1	0.96	0.61	1.14	2.66	77	46	31	60	1.09

Table 2 (continued)

Name	Particle volume (cm ³)	Bulk density (g/cm ³)	Skeletal density (g/cm ³)	Solid density (g/cm ³)	Total porosity (vol%)	Connected porosity (vol%)	Isolated porosity (vol%)	Pore connectivity (vol%)	Saturation density (g/cm ³)
SNB3 snkLb 4mm-1	0.09 ^b	0.70	1.05	2.61	73	34	40	46	1.04
SNB3 snkLb 4mm-2	0.09 ^b	0.69	1.06	2.61	74	36	38	48	1.05
SNB3 snkLb 2mm	0.01 ^b	0.75	1.08	2.57	71	30	40	43	1.06
SNB3 snkLb 1mm	0.001 ^b	0.70	1.35	2.53	72	48	24	66	1.19

^a Lines in italics represent ranges and averages in a bracket

^b Particle volume calculated from sphere volume equivalent to median Φ scale in the sieve class

^c Not determined

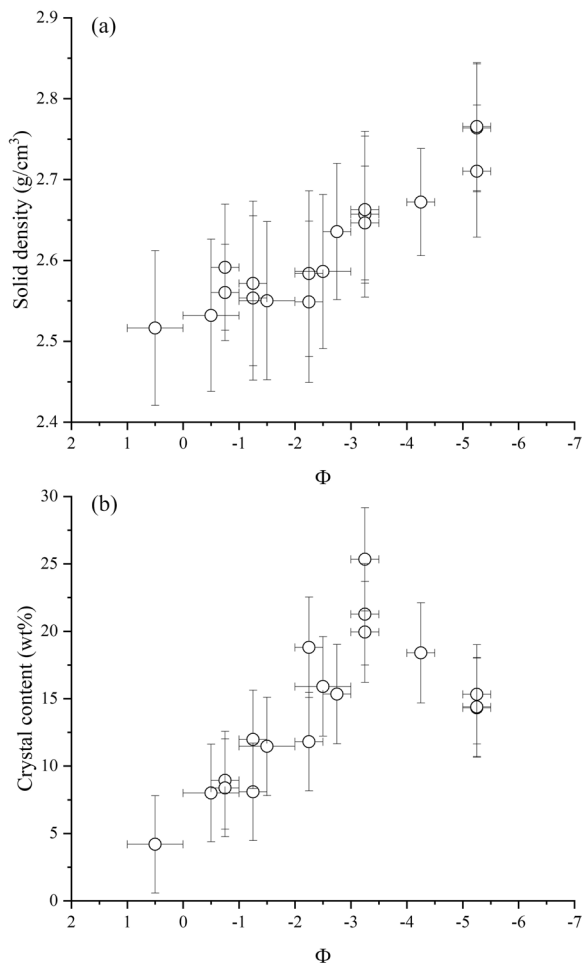


Fig. 5 **a** Solid density and **b** crystal content vs. particle size of the floating pumice particles

single-particle samples, the particle diameter was calculated from its measured volume assuming a sphere with equivalent volume, and converted to the Φ scale. For

multiparticle samples, the median Φ values of the sieve class were adopted. The error of solid density was simply and conservatively set to 0.1 g/cm³ for all particles, considering scattered data with errors in Fig. 5a. Equation (4) was also applied to calculate the solid density of the sunken pumice.

6.5 Total, connected and isolated porosities

The total and connected porosities of the pumice were calculated by applying the bulk (Sect. 6.2), skeletal (Sect. 6.3) and solid (Sect. 6.4) densities to Eq. (1) and (2), respectively (Table 2 and Table S1). By applying the total and connected porosities to Eq. (3), the isolated porosity of the pumice can be calculated (Table 2 and Table S1).

The total porosities of floating and sunken pumice are 73–91 vol%, with an average of 78 vol%, and 71–79 vol%, with an average of 75 vol%, respectively (Fig. 6a). The connected porosities of floating and sunken pumice are 20–80 vol%, with an average of 34 vol%, and 30–55 vol%, with an average of 44 vol%, respectively (Fig. 6b). Owing to the decrease in the skeletal volume, the errors in the connected porosity measured as a single-particle sample increased with decreasing particle volume. The isolated porosities of floating and sunken pumice are 11–58 vol%, with an average of 44 vol%, and 24–40 vol%, with an average of 31 vol%, respectively (Fig. 6c). A particle with uniquely high total porosity of 91 vol% and connected porosity of 79 vol%, corresponding to the only floating pumice particle with a skeletal density higher than that of seawater (Fig. 4b) was observed.

6.6 Bulk rock composition

All bulk rock composition (Table S4) is shown on an K₂O-SiO₂ diagram normalized on an Na₂O-free basis (Fig. 7a) and K₂O on an Na₂O-free basis- Φ diagram

Table 3 Solid density and crystal content of sieved samples of floating pumice erupted in the Fukutoku-Oka-no-Ba 2021 eruption

Name	Particle size (Φ)	Mass ^a (g)	Volume ^a (cm ³)	Solid density (g/cm ³)	Error (g/cm ³)	Crystal content (wt%)	Error (wt%)
SNB5flt – 5.0φ	– 5.0 to – 5.5	4.34	1.57	2.76	0.08	15	4
SNB5flt – 5.0φ	– 5.0 to – 5.5	4.05	1.49	2.71	0.08	14	4
SNB5flt – 5.0φ	– 5.0 to – 5.5	4.35	1.57	2.77	0.08	14	4
SNB1&2flt – 4.0φ	– 4.0 to – 4.5	4.86	1.82	2.67	0.07	18	4
SNB1&2flt – 3.0φ	– 3.0 to – 3.5	3.10	1.17	2.66	0.10	25	4
SNB1&2flt – 3.0φ – 2	– 3.0 to – 3.5	4.48	1.69	2.65	0.07	20	4
YGC3flt – 3.0φ	– 3.0 to – 3.5	3.51	1.32	2.66	0.09	21	4
IKB1flt – 2.5φ	– 2.5 to – 3.0	3.71	1.41	2.64	0.08	15	4
SNB1&2flt – 2φ	– 2.0 to – 3.0	3.16	1.22	2.59	0.10	16	4
YGC3flt – 2.0φ	– 2.0 to – 2.5	2.94	1.14	2.58	0.10	19	4
IKB1flt – 2.0φ	– 2.0 to – 2.5	2.93	1.15	2.55	0.10	12	4
SNB1&2flt – 1φ	– 1.0 to – 2.0	2.99	1.17	2.55	0.10	11	4
YGC3flt – 1.0φ	– 1.0 to – 1.5	2.92	1.14	2.57	0.10	12	4
IKB1flt – 1.0φ	– 1.0 to – 1.5	2.89	1.13	2.55	0.10	8	4
YGC3flt – 0.5φ	– 0.5 to – 1.0	3.87	1.49	2.59	0.08	9	4
YGC1flt – 0.5φ	– 0.5 to – 1.0	4.95	1.93	2.56	0.06	8	4
SNB1&2flt 0φ	0.0 to – 1.0	3.07	1.21	2.53	0.09	8	4
SNB1&2flt 1φ	1.0 to 0.0	2.98	1.18	2.52	0.10	4	4

^a Mass and volume of powder samples used in the solid density measurements

(Fig. 7b). The normalization on an Na₂O-free basis was applied to reduce the effects of inadequate cleaning of sea salt in the samples (Section S2.2 in the Supplementary Materials). Data on the FOB gray pumice from Yoshida et al. (2022b) were shown with the same normalization on an Na₂O-free basis. Data on pumice particles with a diameter of – 2 to – 5 Φ (from 4 to 32 mm in diameter) overlap with or are close to those of Yoshida et al. (2022b). As the particle size decreases from – 2 to 1 Φ (from 4 to 0.5 mm in diameter), the K₂O content increases with the SiO₂ content and Φ (Fig. 7).

6.7 Crystal and groundmass glass composition

The average chemical compositions of crystal phases with modal fractions in whole crystals and assumed crystal densities to convert area fraction to weight fraction are shown in Table S5. Although there was no K₂O-rich phase, plagioclase contained trace amount of K₂O because of its high albite content. The compositions of the groundmass glasses are listed in Table S5. The crystal and groundmass compositions were normalized on an Na₂O-free basis for mass balance calculations to estimate the crystal content. The whole crystal and groundmass compositions are also plotted on the SiO₂–K₂O diagram on an Na₂O-free basis as a graphical expression of the mass balance (Fig. 7a).

6.8 Crystal size and content

We estimated the typical crystal size by analyzing back-scattered electron and elemental images of pumice cross sections with an area of 6.2–7.2 cm². The area of the individual crystal was approximated as an ellipse using the ImageJ software, and the crystal size was defined as the median value between the major and minor diameters of the ellipse. The size of the aggregated crystals was regarded as a grain of crystal. The crystal size distributions of the five gray pumice samples are shown in Fig. 8. Crystals with median diameters of 100 to 3000 μm account for >90% of the total crystals, indicating that most crystals should be called phenocrysts in the light of the definition summarized in Takeuchi et al. (2021).

The crystal content was based on a mass balance calculation for the K₂O content on an Na₂O free basis among bulk rock, glass, and crystals (Fig. 5b). Results showed that the crystal content decreased from 25 to 5 wt% as the particle size of the floating pumice decreased. Owing to the slightly higher outlier data at – 3.0 Φ (8 mm in diameter), it appears as if the maxima of the crystal content (ca. 25 wt%) were considered at – 3.0 Φ. In addition, two – 3.0 Φ data points with a lower crystal content (ca. 20 wt%) were present. Considering errors in crystal content, the higher data at – 3.0 Φ may be due to the heterogeneity in the crystal content visible at pumice particle sizes close to the maximum crystal size.

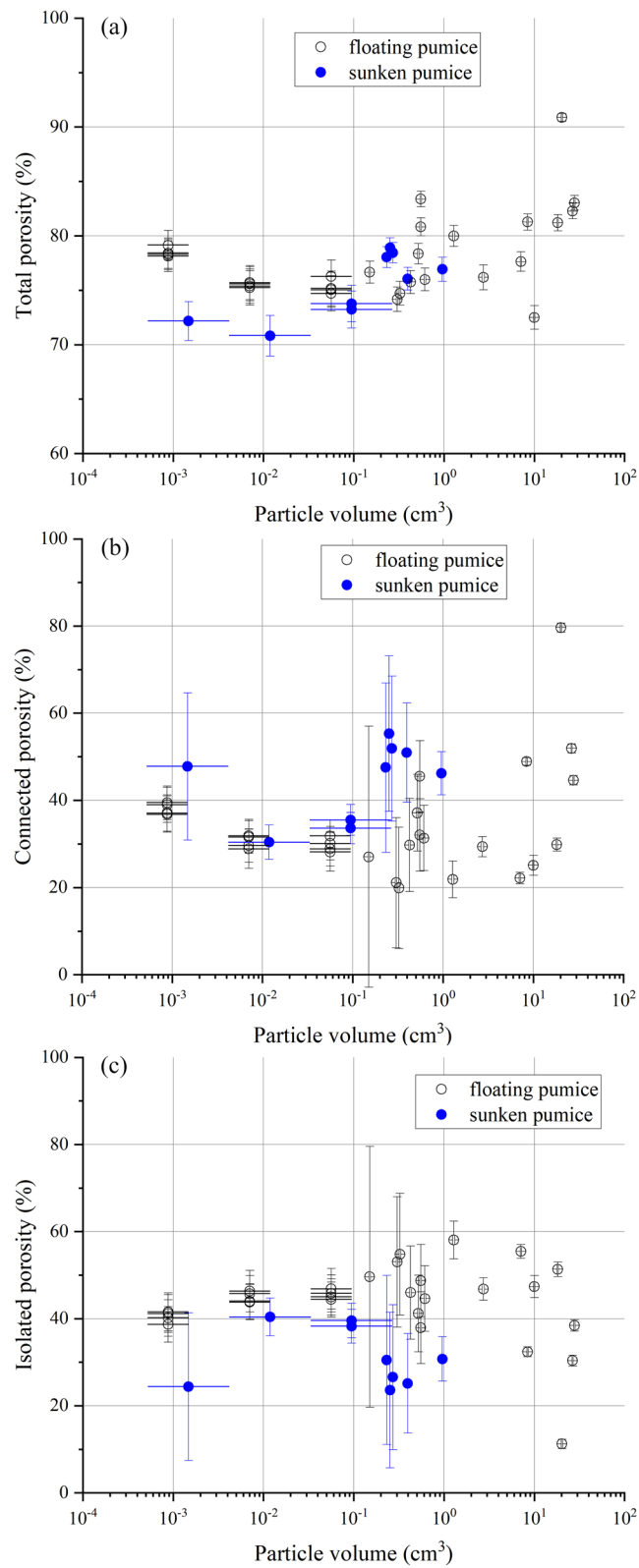


Fig. 6 **a** Total, **b** connected, and **c** isolated porosities versus particle volume

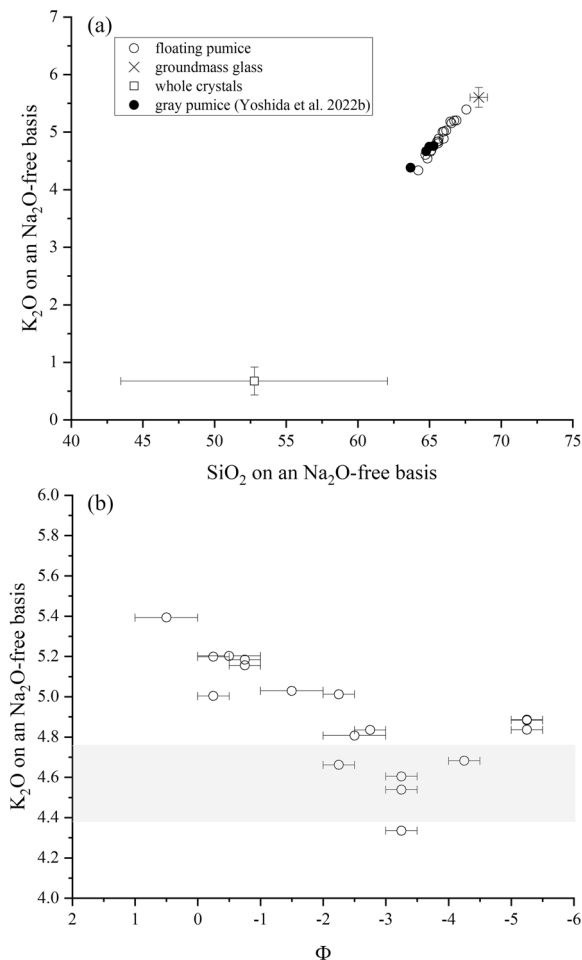


Fig. 7 **a** K₂O vs. SiO₂ contents on an Na₂O-free basis. This figure shows mass balance among the bulk rock composition of the sieved FOB 2021 floating pumice (open circles), averaged composition of groundmass glass (cross), and averaged composition of whole crystals (square). Solid circles represent bulk rock composition of the gray pumices from Yoshida et al. (2022b). **b** K₂O content on an Na₂O free basis vs. particle size of sieved floating pumice. Shaded range represent bulk rock composition of the gray pumices from Yoshida et al. (2022b)

7 Discussion

7.1 Mostly unsinkable and only a few sinkable pumices in the floating pumice

Based on the measured porosities, the saturation density was calculated to examine the floatability of the pumice in seawater (Fig. 9). The saturation density is defined as the density assuming that the connected pores of the pumice are saturated with seawater, assuming that the density of seawater is 1.025 g/cm³, based on Wadachi (1987). Most floating pumice particles have saturation densities lower than that of seawater, and are thus unsinkable. One floating pumice particle with a saturation density higher than that of seawater is expected to

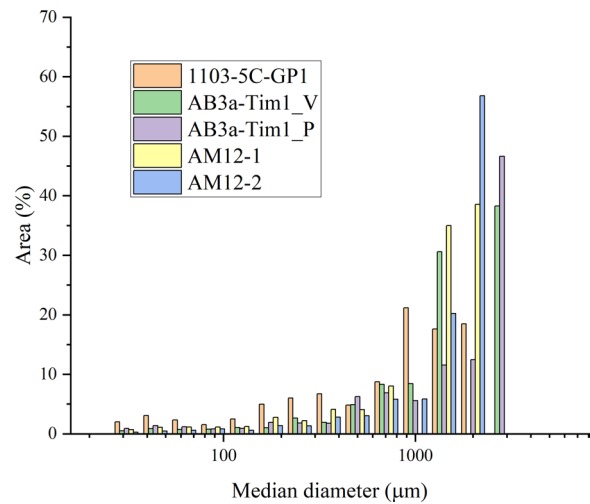


Fig. 8 Crystal size distribution in the centimeter-sized FOB pumices. Median diameter indicates the median value between the long and short axes of ellipses fitted to crystals in the sections

eventually sink once the air trapped in the connected pores is lost (Fauria et al. 2017), and is thus sinkable. The proportion of unsinkable and sinkable pumices in floating pumice particles is difficult to quantify precisely, and can only be roughly estimated. During the sample selection of a floating pumice particle, it is unknown whether the pumice is sinkable or unsinkable. Therefore, the sample selection in this study was random. Under the random selection conditions, only one sinkable pumice was found among the 26 samples. This suggests that, in the studied particle volume range, only a small quantity of the sinkable pumice floated with the help of trapped air in the connected pore.

The relationship between skeletal density and seawater density essentially determines the unsinkable or sinkable pumice (Fig. 4b). If a pumice particle has a skeletal density less than that of seawater, it should be considered unsinkable. Therefore, the determination of unsinkable or sinkable pumice can be performed based solely on the skeletal density, as measured by the gas displacement method. Despite the availability of connected porosity data in many previous studies, skeletal density data are yet to be explicitly stated. Therefore, we emphasize that skeletal density should be explicitly shown as an effective measure of eventual pumice floatability (sinkable or unsinkable).

7.2 Influence of crystals on pumice floatability and size

Porosimetric and petrological data indicate that petrological properties influence the relationship between floatability and pumice size. When the pumice size becomes down and close to the typical crystal size (Fig. 8), the

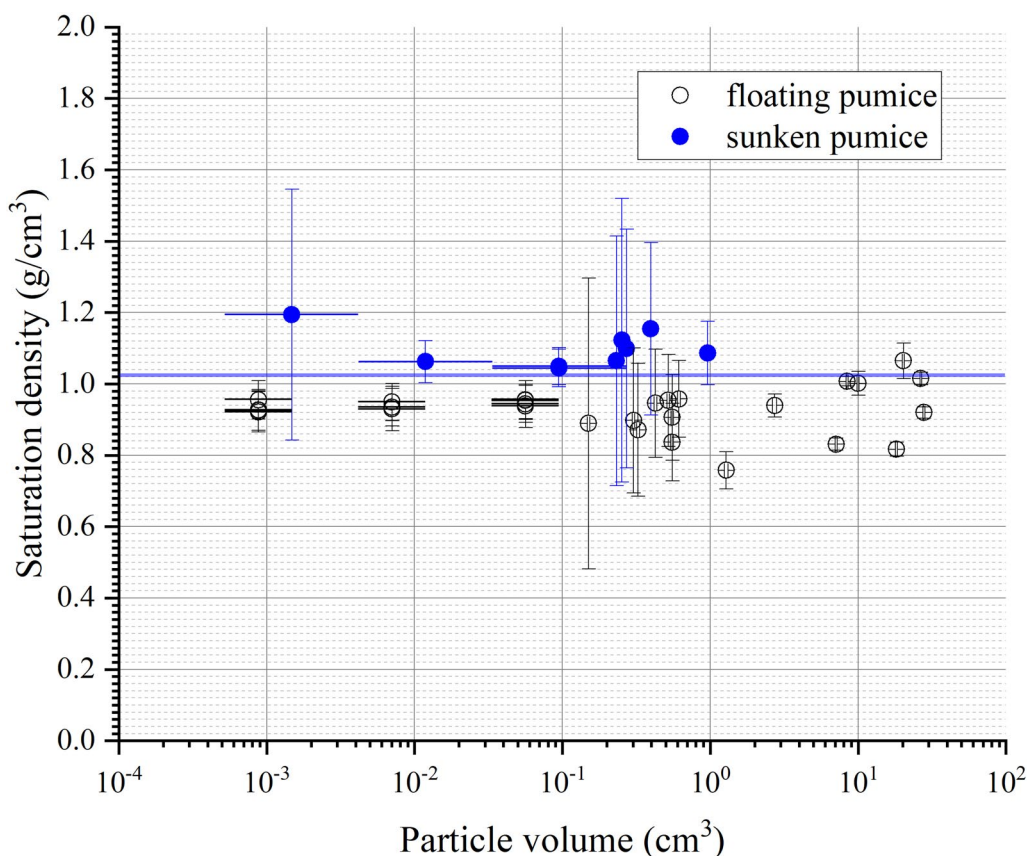


Fig. 9 Saturation density vs. particle volume. A horizontal blue line indicates an assumed range in the density of seawater (1.02 to 1.03 g/cm³), based on Wadachi (1987)

crystal content of floating pumice decreases with pumice particle size (Fig. 5b). We interpreted that pumice containing fewer crystals and a more pumiceous groundmass glass could selectively survive as floating pumice on the sea surface when the pumice size approaches the typical crystal size. The pumiceous groundmass glass plays an important role in reducing the skeletal density as isolated pores exist in the glass. In contrast, we interpreted that crystal-rich, millimeter-sized pumice particles or mostly crystal fragments with still pumiceous glass around sank into the sea, and were not observed as floating pumice particles. The almost absence of floating pumice smaller than 1.0 Φ (0.5 mm in diameter) (Fig. 3) suggests that almost all pumices smaller than 1.0 Φ sank due to losing isolated pores and were not observed as floating pumice particles.

7.3 Comparison with other natural and experimental pumices

Comparison with existing porosity data for natural pumice originating from subaerial and submarine eruptions and for experimental pumice from decompression

experiments provides an interpretation that rapid quenching of the FOB 2021 magma with relatively low to moderate crystal content by the seawater produced unsinkable pumice with abundant isolated porosity.

Figure 10a shows the relationship between total porosity and pore connectivity for pumices from the FOB 2021 and other submarine eruptions. Pore connectivity is defined as the connected porosity divided by the total porosity (Colombier et al. 2017a). The permeable porosity measured using water pycnometry in Kato (1987, 1988) was regarded as connected porosity. The FOB 2021 floating pumice particles have high total porosity and low pore connectivity, similar to part of the beached pumice of the Iriomote 1924 (Kato 1987) and FOB 1986 eruptions (Kato 1988), and the raft pumice (RP) of the Havre 2012 eruption (Manga et al. 2018; Mitchell et al. 2021). However, sinkable pumice particles with high total porosity and pore connectivity were common in the raft pumice of the Havre 2012 eruption. The FOB 2021 sunken pumice particles were plotted in the region between the raft pumice and ash-lapilli-block deposits (ALB) sampled on the sea floor proximal

to the vent of the Havre 2012 eruption. Incorporating the compiled data (subaerial pumice and scoria) from Colombier et al. (2017a), Fig. 10a shows that most subaerial pumice and scoria have high pore connectivity of more than 70% and are plotted in the region of sinkable pumice and quite different from the FOB 2021 unsinkable pumice and other unsinkable pumices from submarine eruptions, as noted in a study of the Havre 2012 eruption (Mitchell et al. 2021).

Data of experimental pumices quenched in the decompression experiments of vesiculating magmas are also plotted on the total porosity-pore connectivity diagram with data on pumice of FOB 2021 (Fig. 10b). The total and connected porosities were measured for quenched samples of vesiculated, hydrous silicic melts without crystals (Takeuchi et al. 2009) or with crystals (Graham et al. 2023). The crystal-free samples with 70–80 vol% total porosity (Takeuchi et al. 2009) had pore connectivity in the region of unsinkable pumice, which is close to data on pumice of FOB 2021 (Fig. 10b). The pore connectivity of crystal-free samples rapidly increased at approximately 80 vol% total porosity, and those with > 80 vol% total porosity were plotted in the region of sinkable pumice. Figure 10b also suggests the influence of crystals in the magma on the floatability of the pumice. Colombier et al. (2022) predicted the influence of crystals on pore connectivity by a model analysis. Graham et al. (2023) performed experiments on crystal-bearing rhyolitic magma with up to 40 vol% crystals. For crystal-rich pumices (40 vol% crystal content), the pore connectivity gradually increased with an increase in the total porosity from 20 to 70 vol%. Graham et al. (2023) interprets that the increase in crystal content causes the reduction in interstitial melt available for bubble expansion, resulting in the forced connection among bubbles (pores) at lower total porosity. The total porosity-pore connectivity relationship for crystal-rich pumices varied in the condition of producing sinkable pumice and can not enter the condition of unsinkable pumice. For pumice with moderate crystal content (20 vol% crystal content), the relationship between total porosity and pore connectivity approaches

the boundary separating the condition and appears to enter the region of unsinkable pumice. Considering that the crystal content of FOB 2021 pumices > 4 Φ (16 mm in diameter), larger compared with the typical crystal size shown in Sect. 6.8, shows a more representative crystal content in the magmas, the magmas of the FOB 2021 eruption have a crystal content of < 20 wt% (Fig. 5b). Assuming that the glass and whole crystal density are 2.5 and 3.0 g/cm³, based on solid density of 1 Φ (Table 3) and modal fractions in whole crystals (Table S5), respectively, a crystal content of approximately 20 wt% can be converted to approximately 17 vol%. This low to moderate crystal content in the FOB 2021 magma, together with adequate porosimetric properties, may contribute to favorable conditions to produce abundant, millimeter-sized, unsinkable pumice.

Generally, in decompression experiments, the sample is kept at a high temperature and pressure and then decompressed to the targeted pressure at various decompression rates. The decompressed magmas undergo vesiculation, including bubble nucleation, growth, coalescence, and shape relaxation. Finally, the samples are quenched for a much shorter time than that during a natural eruption process. Based on a study of natural subaerial pumices, Gardner et al. (1996) concluded that the delayed expansion of pumice occurs in the range of melt viscosities in subaerial eruptions. Delayed expansion can cause the isolated pores to expand and transform into connected pores. In contrast, submarine eruptions may have effectively quenched vesicular magmas, as in decompression experiments, resulting in producing more isolated pores in the pumice because delayed expansion after fragmentation can be suppressed (Rotella et al. 2015). Figure 10 shows that pumices from subaerial eruptions can float as air-trapped floating pumices (sinkable pumices) owing to their high connected porosity. Such subaerial pumices are expected to sink after a finite floatation time, depending on the pore structure and particle size (Manville et al. 1998; Fauria et al. 2017). Maeno et al. (2022) interpreted that most of the FOB 2021 pumice were not transported by eruption plume in the atmosphere but rose from the

(See figure on next page.)

Fig. 10 **a** Pore connectivity vs. total porosity. Open and blue solid circles represent floating and sunken pumices, respectively. Crosses, open squares, solid squares, open diamonds, and open triangles represent pumice data for the Havre 2012 ALB (ash-lapilli block) sampled on the seafloor (Mitchell et al. 2021), the Havre 2012 RP (raft pumice; Manga et al. 2018; Mitchell et al. 2021), Shinkai pumice sampled on the seafloor (Kato 1987), the Iriomote 1924 beached pumice (Kato 1987), and the Fukutoku-Oka-no-Ba 1986 beached pumice (Kato 1988), respectively. **b** Pore connectivity vs. total porosity. Open and blue solid circles represent floating and sunken pumices, respectively. Red crosses, open squares, open triangles, open diamonds, gray solid squares, and gray solid triangles represent data for the decompression experiments at a crystal-free condition (Takeuchi et al. 2009), and wollastonite 20%, corundum and wollastonite 20%, corundum 20%, wollastonite 40%, and corundum and wollastonite 40% conditions (Graham et al. 2023). In (a) and (b), gray dots indicate pore connectivity and total porosity of subaerial pumice and scoria compiled by Colombier et al. (2017a). In (a) and (b), solid and broken lines separate the conditions of unsinkable and sinkable pumices with a solid density of 2.8 and 2.5 g/cm³, respectively, assuming that the density of seawater is 1.025 g/cm³, based on Wadachi (1987)

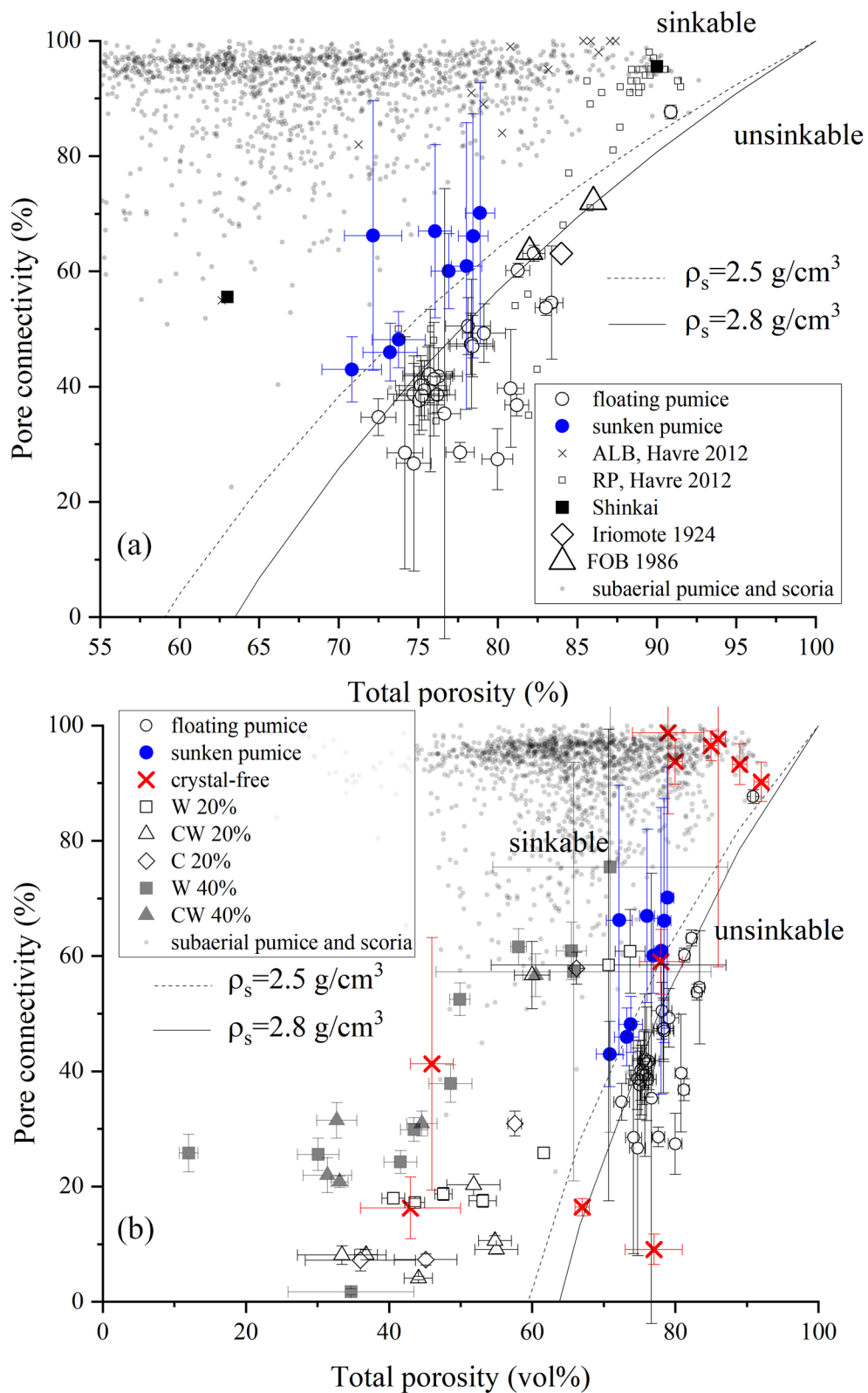


Fig. 10 (See legend on previous page.)

submarine vent to the sea surface. This interpretation is consistent with the porosimetric characteristics of floating pumices of FOB 2021 containing abundant isolated pores, which suggests well-quenching and suppression of delayed expansion after fragmentation.

Considering these experimental results, the conditions for producing unsinkable pumice may be narrowly limited in the case of submarine eruption by magmas with low to moderate crystal content that are quenched at a water depth where high total porosity and relatively low pore connectivity is achieved. Crystal-rich, experimental pumices have a higher pore connectivity at the same total porosity (Fig. 10b), suggesting that sinkable pumice with high pore connectivity can be produced even during submarine eruptions. Consistently with this, the magma that produced large-magnitude pumice rafts in the Havre 2012 eruption was of a crystal-poor nature (Carey et al. 2018).

8 Conclusions

A porosity measurement technique for millimeter-to-centimeter-sized pumice particles was established and applied to drifting pumice that erupted during the FOB 2021 eruption. The total, connected, and isolated porosities with errors were obtained for floating and sunken pumice particles. As for the floating pumices from submarine eruptions studied previously, most floating pumice particles are rich in isolated porosity (> 30 vol%) and are thus unsinkable, even when the pumice size reaches the millimeter scale. This study emphasized that the skeletal density is a useful measure of pumice floatability (sinkable or unsinkable). As the particle size decreases, crystals are lost from the floating pumice particles, suggesting that the particle size of the floating pumice is affected by the petrological properties (crystal content and size). A comparison with natural pumices from subaerial eruptions and experimental pumices from magma decompression experiments suggests that FOB 2021 pumices contain abundant isolated pores due to the suppression of expansion after fragmentation by quenching in seawater, and that the relatively low to moderate crystal content (< 17 vol%) may contribute to favorable condition to produce abundant, millimeter-sized, unsinkable pumice. The floatability of unsinkable pumice will be changed if its pore structure is changed. For example, splitting, abrasion, and weathering of pumice can change the isolated pores to connected pores, producing sinkable pumice. However, these processes remain poorly known and are thus important targets in future field and experimental studies. After the 2021 eruption, a dredge survey in a research cruise revealed pyroclastic materials that were deposited on the sea floor in the vicinity of the FOB volcano without long-drifting (Yoshida et al. 2023b).

It is also a future theme to clarify the difference in porosimetric characteristics between the deposited and long-drifting pumice.

Abbreviations

FOB	Fukutoku-Oka-no-Ba
XRF	X-ray fluorescence
WDS	Wavelength dispersive spectroscopy

Supplementary Information

The online version contains supplementary material available at <https://doi.org/10.1186/s40645-024-00652-9>.

Additional file 1.
Additional file 2.
Additional file 3.
Additional file 4.
Additional file 5.
Additional file 6.

Acknowledgements

We thank Ito, H. and Toshida, K. for supporting our field work and valuable discussion, and officials of Kominato fishing port at the Amami-Oshima Island for providing pumice sample. We thank Editage (www.editage.jp) for English language editing. We also thank Colombier, M. and an anonymous reviewer for giving comments to improve the manuscript and Nakagawa, M. for editorial handling.

Author contributions

ST designed the study, conducted field work, collected samples, performed sieve analysis and density measurements, and wrote the manuscript; KI conducted field work, collected samples, performed sieve analysis, density measurements and petrological analysis; SU conducted field work and collected samples; YS conducted field work, collected samples, performed density measurements and petrological analyses. All authors discussed the results and approved the final manuscript.

Funding

This work was funded by Central Research Institute of Electric Power Industry.

Availability of data and materials

The datasets supporting the conclusions of this article are included within the article and its additional files.

Declarations

Competing interests

The author declares no competing interests.

Received: 21 December 2023 Accepted: 21 August 2024

Published online: 04 September 2024

References

- Akiyama Y, Okada T, Yuhara T (2022) Observations of mobile macro-epifauna on pumice rafts generated by Fukutoku-Oka-no-Ba volcano in Oku Port Okinawa Prefecture. *Aquat Anim* 2022:AA2022-AA2113. https://doi.org/10.34394/aquaticanimals.2022.0_AA2022-13
- Asami M, Takahashi C (2023) Drift prediction of pyroclasts released through the volcanic activity of Fukutoku-Okanoba into the marine environment. *Mar Pollut Bull* 186:114402. <https://doi.org/10.1016/j.marpolbul.2022.114402>

- Bryan SE, Cook AG, Evans JP, Hebden K, Hurrey L, Colls P, Jell JS, Weatherly D, Finn J (2012) Rapid, long-distance dispersal by pumice rafting. *PLoS ONE* 7:e40583. <https://doi.org/10.1371/journal.pone.0040583>
- Carey RJ, Soule SA, Manga M, White JDL, McPhie J, Wysoczanski R, Jutzeler M, Tani K, Fornari D, Caratori-Tontini F, Houghton BF, Mitchell SJ, Ikegami F, Conway C, Murch A, Fauria K, Jones M, Cahalan R, McKenzie W (2018) The largest deep-ocean silicic volcanic eruption of the past century. *Sci Adv* 4(1):e1701121. <https://doi.org/10.1126/sciadv.1701121>
- Chang YLK, McIntosh IM, Miyama T, Miyazawa Y (2023) Projection of August 2021 pumice dispersion from the Fukutoku-Oka-no-Ba eruption in the western North Pacific. *Sci Rep* 13:3945. <https://doi.org/10.1038/s41598-023-31058-0>
- Colombier M, Wadsworth FB, Gurioli L, Scheu B, Kueppers U, Di Muro A, Dingwell DB (2017a) The evolution of pore connectivity in volcanic rocks. *Earth Planet Sci Lett* 62:99–109. <https://doi.org/10.1016/j.epsl.2017.01.011>
- Colombier M, Gurioli L, Druitt TH, Shea T, Boivin P, Miallier D, Cluzel N (2017b) Textural evolution of magma during the 9.4-ka trachytic explosive eruption at Kilian Volcano, Chaîne des Puys, France. *Bull Volcanol* 79:17. <https://doi.org/10.1007/s00445-017-1099-7>
- Colombier M, Bernard B, Wright H, Le Pennec JL, Cáceres F, Cimarelli C, Heap MJ, Samaniego P, Vasseur J, Dingwell DB (2022) Conduit processes in crystal-rich dacitic magma and implications for eruptive cycles at Guagua Pichincha volcano. *Ecuador Bull Volcanol* 84:105. <https://doi.org/10.1007/s00445-022-01612-1>
- Fauria KE, Manga M, Wei Z (2017) Trapped bubbles keep pumice afloat and gas diffusion makes pumice sink. *Earth Planet Sci Lett* 460:50–59. <https://doi.org/10.1016/j.epsl.2016.11.055>
- Fauria KE, Jutzeler M, Mittal T, Gupta AK, Kelly LJ, Rausch J, Bennartz R, Delbridge B, Retailleau L (2023) Simultaneous creation of a large vapor plume and pumice raft by the 2021 Fukutoku-Oka-no-Ba shallow submarine eruption. *Earth Planet Sci Lett* 609:118076. <https://doi.org/10.1016/j.epsl.2023.118076>
- Gardner J, Thomas R, Jaupart C, Tait S (1996) Fragmentation of magma during Plinian volcanic eruptions. *Bull Volcanol* 58:144–162. <https://doi.org/10.1007/s004450050132>
- Graham NA, Larsen JF, Tasa KY, deGraffenried RL, Cashman KV, McCartney KN (2023) Controls of crystal shape on degassing mechanisms in crystal-rich magmas with rhyolitic groundmass melts. *Earth Planet Sci Lett* 601:117891. <https://doi.org/10.1016/j.epsl.2022.117891>
- Heinrich M, Cronin SJ, Torres-Orozco R, Colombier M, Scheu B, Pardo N (2020) Micro-porous pyroclasts reflecting multi-vent basaltic-andesite Plinian eruptions at Mt. Tongariro, New Zealand. *J Volcanol Geotherm Res* 401:106936. <https://doi.org/10.1016/j.jvolgeores.2020.106936>
- Heki K, Fujimoto T (2022) Atmospheric modes excited by the 2021 August eruption of the Fukutoku-Okanoba volcano, Izu–Bonin Arc, observed as harmonic TEC oscillations by QZSS. *Earth Planets Space* 74:27. <https://doi.org/10.1186/s40623-022-01587-5>
- Houghton BF, Wilson CJN (1989) A vesicularity index for pyroclastic deposits. *Bull Volcanol* 51:451–462. <https://doi.org/10.1007/BF01078811>
- Iskandar MR, Park YG, Kim K, Jin H, Seo S, Kim YH (2023) Tracking the pumice rafts from the Fukutoku-Okanoba submarine volcano with satellites and a Lagrangian particles trajectory model. *Mar Pollut Bull* 193:115254. <https://doi.org/10.1016/j.marpolbul.2023.115254>
- Ito K, Kato S, Takahashi M, Saito A (2011) Volcanic topography of Fukutoku-Oka-no-Ba volcano in Izu-Ogasawara Arc after 2010 eruption. *Rep Hydrogr Oceanogr Res* 47:9–13 **(in Japanese with English abstract)**
- Japan Meteorological Agency (2021a) Fukutoku-oka-no-ba. In: The 149th meeting of the coordinating committee for prediction of volcanic eruption (Part 2 of 4) Fukutoku-oka-no-ba. (Title was translated by the authors). https://www.data.jma.go.jp/svd/vois/data/tokyo/STOCK/kaisei/tsu/CCPVE/shiroyo/149/149_2-4.pdf
- Japan Meteorological Agency (2021b) Monthly volcanic activity reports of Fukutoku-Oka-no-Ba, 2021 August. https://www.data.jma.go.jp/svd/vois/data/tokyo/STOCK/monthly_v-act_doc/tokyo/21m08/331_21m08.pdf (Title was translated by Yoshida et al., 2022b).
- Jutzeler M, Marsh R, Carey R, White JDL, Talling PJ, Karlstrom L (2014) On the fate of pumice rafts formed during the 2012 Havre submarine eruption. *Nat Commun* 5:3660. <https://doi.org/10.1038/ncomms4660>
- Jutzeler M, Marsh R, van Sebille E, Mittal T, Carey RJ, Fauria KE, Manga M, McPhie J (2020) Ongoing dispersal of the 7 August 2019 pumice raft from the Tonga Arc in the Southwestern Pacific Ocean. *Geophys Res Lett* 47:1–3. <https://doi.org/10.1029/2019GL086768>
- Kaneta S, Chiba T (2022) Brief summary of floating pumice caused by Fukutoku-Oka-no-Ba submarine volcanic eruption. *J Remote Sens Soc Jpn* 42(3):96–198. <https://doi.org/10.11440/rssj.42.196>
- Kato Y (1987) Woody pumice generated with submarine eruption. *J Geol Soc Jpn* 93(1):11–20.2. <https://doi.org/10.5575/geosoc.93.11>
- Kato Y (1988) Gray pumices drifted from Fukutoku-Oka-no-Ba to the Ryukyu Islands. *Bull Volcanol Soc Jpn* 33:21–30. https://doi.org/10.18940/kazanc.33.1_21. **(in Japanese with English abstract)**
- Konoo T, Naruo H, Miyabuchi Y (2022) Drifting situation of pumices discharged from the 2021 eruption of Fukutoku-Oka-no-Ba volcano: cases at Osumi Peninsula in Kagoshima Prefecture, Southern Part of Miyazaki Prefecture, Tanegashima and Amami Oshima Islands. *Bull Volcanol Soc Jpn* 67:401–408. https://doi.org/10.18940/kazan.67.3_401
- Krumbein WC (1934) Size frequency distributions of sediments. *J Sediment Res* 4(2):65–77. <https://doi.org/10.1306/D4268EB9-2B26-11D7-864800102C1865D>
- Maeno F, Kaneko T, Ichihara M, Suzuki YJ, Yasuda A, Nishida K, Ohminato T (2022) Seawater-magma interactions sustained the high column during the 2021 phreatomagmatic eruption of Fukutoku-Oka-no-Ba. *Commun Earth Environ* 3:60. <https://doi.org/10.1038/s43247-022-00594-4>
- Manga M, Fauria KE, Lin C, Mitchell SJ, Jones M, Conway CE, Degruyter W, Hoseni B, Carey R, Cahalan R, Houghton BF (2018) The pumice raft-forming 2012 Havre submarine eruption was effusive. *Earth Planet Sci Lett* 489:49–58. <https://doi.org/10.1016/j.epsl.2018.02.025>
- Manville V, White JDL, Houghton BF, Wilson CJN (1998) The saturation behaviour of pumice and some sedimentological implications. *Sediment Geol* 119:5–16. [https://doi.org/10.1016/S0037-0738\(98\)00057-8](https://doi.org/10.1016/S0037-0738(98)00057-8)
- McManus DA (1963) A criticism of certain usage of the phi-notation. *J Sediment Res* 33(3):670–674. <https://doi.org/10.1306/74D70EED-2B21-11D7-864800102C1865D>
- Michol KA, Russell JK, Andrews GDM (2008) Welded block and ash flow deposits from Mount Meager, British Columbia, Canada. *J Volcanol Geotherm Res* 169:121–144. <https://doi.org/10.1016/j.jvolgeores.2007.08.010>
- Minami H, Tani K (2023) The Fukutoku Volcanic Complex: Implications for the northward extension of Mariana rifting and its tectonic controls on arc volcanism. *Mar Geol* 457:106996. <https://doi.org/10.1016/j.margeo.2023.106996>
- Mitchell SJ, Fauria KE, Houghton BF, Carey RJ (2021) Sink or float: micro-textural controls on the fate of pumice deposition during the 2012 submarine Havre eruption. *Bull Volcanol* 83:80. <https://doi.org/10.1007/s00445-021-01497-6>
- Nagayama A, Izaki T (2022) The experiments of pumice stone drifting of the moving process in the wind tunnel. *J Jpn Soc Civ Eng Ser B3 Ocean Eng* 78:l_865–l_870. https://doi.org/10.2208/jscejoe.78.2_l_865
- Nakamura M, Otaki K, Takeuchi S (2008) Permeability and pore-connectivity variation of pumices from a single pyroclastic flow eruption: implications for partial fragmentation. *J Volcanol Geotherm Res* 176:302–314. <https://doi.org/10.1016/j.jvolgeores.2008.04.011>
- Nakata Y, Uda T, Takahashi K, Noshi Y (2022) Field observation of deposition of pumice around detached breakwaters—an example of Ogimi coast on Okinawa Island. *J Jpn Soc Civ Eng Ser B3 Ocean Eng* 78:l_733–l_738. https://doi.org/10.2208/jscejoe.78.2_l_733
- Nishikawa H, Kuwatani T, Tada N, Watanabe HK (2023) Simulated distributions of pumice rafts in Japan following eruptions at volcanic islands and submarine volcanoes. *Prog Earth Planet Sci* 10:21. <https://doi.org/10.1186/s40645-023-00552-4>
- Noshi Y, Uda T, Takahashi K, Nakata Y (2022) Field observation of deposition of pumice produced by eruption of underwater volcano in 2021-UAV observation around Yagaji fishing port-. *J Jpn Soc Civ Eng Ser B3 Ocean Eng* 78:l_721–l_726. https://doi.org/10.2208/jscejoe.78.2_l_721
- Ohno Y, Iguchi A, Ijima M, Yasumoto K, Suzuki A (2022) Coastal ecological impacts from pumice rafts. *Sci Rep* 12:11187. <https://doi.org/10.1038/s41598-022-14614-y>
- Oikawa T, Ikegami F, Watanabe S (2023) Eruption Styles and Source Volcanoes for Drifting Pumice Deposited along the Nansai Islands, Southwest Japan. *Bull Volcanol Soc Jpn* 68:171–187. https://doi.org/10.18940/kazan.68.3_171. **(in Japanese with English Abstract)**

- Pardo N, Cronin S, Palmer A, Procter J, Smith I (2012) Andesitic Plinian eruptions at Mt. Ruapehu: quantifying the uppermost limits of eruptive parameters. *Bull Volcanol* 74:1161–1185. <https://doi.org/10.1007/s00445-012-0588-y>
- Rotella MD, Wilson CJN, Barker SJ, Schipper CI, Wright IC, Wysoczanski RJ (2015) Dynamics of deep submarine silicic explosive eruptions in the Kermadec arc, as reflected in pumice vesicularity textures. *J Volcanol Geotherm Res* 301:314–332. <https://doi.org/10.1016/j.jvolgeoes.2015.05.021>
- Sasaki T, Katsui Y (1981) Pycnometry of pumice by using glass beads. *Bull Volcanol Soc Jpn* 26:117–118 (in Japanese)
- Sato H, Sakai Y, Kuwamura T (2023) Protective resemblance to floating pumice stones by juveniles of the rough triggerfish *Canthidermis maculata* (Balistidae, Tetraodontiformes). *Ichthyol Res* 70:301–304. <https://doi.org/10.1007/s10228-022-00877-y>
- Shimano T, Nakada S (2006) Vesiculation path of ascending magma in the 1983 and the 2000 eruptions of Miyakejima volcano, Japan. *Bull Volcanol* 68:549–566. <https://doi.org/10.1007/s00445-005-0029-2>
- Ryukyu Shimpo (2021) Large amounts of fish are killed after swallowing pumice stones from undersea volcanic eruption, 14 Okinawan fisheries reeling from the damage as Okinawa and Japan coordinate on removal. October 26, <http://english.ryukyushimpo.jp/2021/10/29/34157/>. Accessed 11 Oct 2023
- Ryukyu Shimpo (2022) Pumice stone removal costs expected to exceed 1.6 billion yen, not including damage to fishing and tourism industries. February 18. <http://english.ryukyushimpo.jp/2022/02/22/34456/>. Accessed 11 Oct 2023
- Yomiuri Shinbun (2021) Pumice: Where is the blue sea? Diving filming at the coast of Onna Village, Okinawa (Japanese title translated by the author). <https://www.yomiuri.co.jp/local/kyushu/news/20211112-OYTNT50027/>. Accessed 23 May 2024
- Shiraki Y, Katayama R, Shinogi C, Ono N (2022) Pumice drift simulation in OKINAWA coastal area. *J Jpn Soc Civ Eng Ser B3 Ocean Eng* 78:I_871-I_876. https://doi.org/10.2208/jscejoe.78.2_I_871
- Takahashi K, Uda T, Noshi Y, Nakata Y (2022) Deposition of pumice on beaches around groins on south Ogimi coast in Okinawa. *J Jpn Soc Civ Eng Ser B3 Ocean Eng* 78:I_727-I_732. https://doi.org/10.2208/jscejoe.78.2_I_727
- Takeuchi S, Tomiya A, Shinohara H (2009) Degassing conditions for permeable silicic magmas: implications from decompression experiments with constant rates. *Earth Planet Sci Lett* 283:101–110. <https://doi.org/10.1016/j.epsl.2009.04.001>
- Takeuchi S, Yoshida K, Miura D, Ito H, Uesawa S (2021) Relationships between magmatic properties and eruption magnitude of explosive eruptions at Japanese arc volcanoes during the last one hundred thousand years. *J Volcanol Geotherm Res* 419:107345. <https://doi.org/10.1016/j.jvolgeoes.2021.107345>
- Usami K, Shinjo R (2022) Drifted pumice stones at Okinawa Prefecture derived from the 2021 August eruption at Fukutoku-Oka-no-Ba submarine volcano. *Bull Okinawa Prefect Mus Art Mus* 15:1–16
- Wadachi K (1987) Encyclopedia of oceanography. Tokyodo, Tokyo, p 589
- Whitham AG, Sparks RSJ (1986) Pumice. *Bull Volcanol* 48:209–223. <https://doi.org/10.1007/BF01087675>
- Yokoyama T, Takeuchi S (2009) Porosimetry of vesicular volcanic products by a water-expulsion method and the relationship of pore characteristics to permeability. *J Geophys Res Solid Earth* 114:B02201. <https://doi.org/10.1029/2008JB005758>
- Yoshida K, Tamura Y, Sato T, Sangmanee C, Puttapreecha R, Ono S (2022a) Petrographic characteristics in the pumice clasts deposited along the Gulf of Thailand, drifted from Fukutoku-Oka-no-Ba. *Geochem J* 56:134–137. <https://doi.org/10.2343/geochemj.GJ22011>
- Yoshida K, Tamura Y, Sato T, Hanyu T, Usui Y, Chang Q, Ono S (2022b) Variety of the drift pumice clasts from the 2021 Fukutoku-Oka-no-Ba eruption Japan. *Isl Arc* 31:e12441. <https://doi.org/10.1111/iar.12441>
- Yoshida K, Maruya Y, Kuwatani T (2022c) Chocolate-chip cookie-like pumice from the 2021 Fukutoku-Oka-no-Ba eruption: views from SNS-related geology. *Jpn Mag Mineral Petrol Sci* 51:220412. <https://doi.org/10.2465/gkk.220412>
- Yoshida K, Miyake A, Okumura SH, Ishibashi H, Okumura S, Okamoto A, Niwa Y, Kimura M, Sato T, Tamura Y, Ono S (2023a) Oxidation-induced nanolite crystallization triggered the 2021 eruption of Fukutoku-Oka-no-Ba, Japan. *Sci Rep* 13:7117. <https://doi.org/10.1038/s41598-023-34301-w>
- Yoshida K, Tamura Y, Sato T, Tanaka E, Tada N, Hamada M, Hanyu T, Chang Q, Ono S (2023b) The proximal volcanoclastic materials of Fukutoku-Oka-no-Ba in the Izu–Bonin arc show contrasting characteristics to the drift pumice of the 2021 eruption. *Isl Arc* 32:e12498. <https://doi.org/10.1111/iar.12498>

Publisher's Note

Springer Nature remains neutral with regard to jurisdictional claims in published maps and institutional affiliations.